

Digital Simulation of Non-Abelian Parafermions in Superconducting Circuits

Hong-Yu Wang^{1,2,3} and Xiong-Jun Liu^{1,2,3,*}

¹*International Center for Quantum Materials and School of Physics, Peking University, Beijing 100871, China*

²*International Quantum Academy, Shenzhen 518048, China*

³*Hefei National Laboratory, Hefei 230088, China*

Parafermions, which can be viewed as a fractionalized version of Majorana modes, exhibit non-Abelian statistics and emerge in topologically ordered systems, while their realization in experiment has been challenging. Here we propose an experimental scheme for the digital simulation of parafermions and their non-Abelian braiding in superconducting circuits by realizing the \mathbb{Z}_d plaquette model on a two-dimensional lattice. Two protocols using quantum circuits and non-destructive measurements are introduced to prepare the ground state, on which the parafermion pairs are created by engineering dislocations. We further develop a generalized code deformation approach to realize the fusion and non-Abelian braiding statistics of parafermion modes, in which the concrete example for $d = 3$ parafermions is studied in detail. We also examine the real parameter regime to confirm the feasibility in superconducting devices. This work extends previous methods for twist defects in superconducting qubits to qudit systems, and may open up a way for parafermion-based high-dimensional topological quantum computing with experimental feasibility.

I. INTRODUCTION

The recent rapid advancement in quantum processors enables simulation of many-body quantum states and exploration of the intriguing physics they exhibit [1–6]. This provides a way to study and manipulate exotic particles that have yet to be realized or are difficult to manipulate in real materials [7–11]. A notable example is the simulation of anyons and topological defects in topologically ordered states (topological orders) [3, 4, 12–15]. In particular, recent progress in digital simulation of twist defects in the \mathbb{Z}_2 toric code model with superconducting qubits demonstrates the fusion rules and (projective) non-Abelian braiding statistics [3, 4]. These efforts contribute to topologically protected quantum information processing and advance the potential realization of topological quantum computing.

Twist defects in the \mathbb{Z}_2 toric code model exhibit non-Abelian statistics of Majorana fermions, which is described by the Ising anyon model [16, 17]. Quantum computing schemes based on Majorana fermions have been widely studied, but their experimental realization in one- or two-dimensional condensed matter systems faces significant challenges [18–46]. More critically, braiding of Majorana fermions alone is insufficient for universal quantum computing [47, 48]. Universal quantum computing schemes based on Majorana fermions require additional non-topological assistance methods, making them not strictly topological [49, 50]. \mathbb{Z}_d parafermions generalize Majorana fermions (which are a special case for $d = 2$) and exhibit more complex non-Abelian braiding statistics [51, 52]. In contrast to Majorana fermions, parafermions can encode multi-level computational units, or qudits, which offer a larger state space for storing and processing information, as well as advantages in re-

ducing circuit complexity and improving algorithm efficiency [53]. Braiding of parafermions allows the generation of the single-qudit Clifford group for any d , and the many-qudit Clifford group for odd d [54]. Fault-tolerant non-Clifford gates are performed by magic state distillation [55–57].

Proposals for realizing parafermions typically involve systems with strong electron-electron interactions, which however pose serious experimental challenges [58–70]. On the other hand, to engineer the topological defects is an alternative general approach for realizing non-Abelian statistics within Abelian topological orders [71]. Furthermore, the braiding of Abelian anyons facilitates performing non-Clifford gate in such phases. This enables a simpler way to explore parafermion defects in Abelian topologically ordered states. A typical class of stabilizer Hamiltonian models that realize these states is the \mathbb{Z}_d plaquette models with qudits on a two-dimensional square lattice, in which certain lattice dislocations realize parafermions [72]. As a stabilizer model, the digital simulation of its ground and excited states with a few quasiparticles is naturally achievable on experimental platforms with coherent control of qudits. Superconducting circuits based on transmons, which have readily addressable higher energy levels, is a well-suited candidate for such a platform [73]. Recent works on superconducting devices have demonstrated high-fidelity single- and two-qudit (qudit with $d = 3$) entangling operations [74–80]. It holds great promise for the preparation and manipulation of high-fidelity ground and excited states of the \mathbb{Z}_d plaquette model with parafermion defects for larger d in superconducting circuits in the near future.

In this work, we propose an experimentally feasible scheme to simulate parafermions and their non-Abelian braiding in superconducting circuits, focusing on the \mathbb{Z}_d plaquette model on a planar surface. We introduce two efficient ground state preparation protocols: one using quantum circuits and the other employing non-destructive measurements. By engineering dislocations

* Corresponding author: xiongjunliu@pku.edu.cn

in the square lattice, pairs of parafermions are created. Through the generalized code deformations, as proposed in the present work, these parafermions are moved on the planar surface, enabling a feasible way for their fusion and braiding operations. The concrete example of $d = 3$ parafermions is studied in detail to demonstrate the fusion and non-Abelian braiding using string operators. The real parameter conditions are examined for the superconducting circuits, with the feasibility of our scheme in experiment being confirmed. We note that while the present simulation is designed for the superconducting devices, it is also compatible with other experimental platforms capable of implementing the gates that we use. Our work provides a theoretical foundation for the imminent digital simulation of parafermions in quantum computing platforms, and may advance high-dimensional quantum information processing and topological quantum computing.

The remainder of the paper is organized as follows. In Sec. II, we introduce the \mathbb{Z}_d plaquette model and its spectrum. In Sec. III, we present the protocol for ground state preparation and parafermion creation. Sections IV and V outline the schemes for realizing the fusion and non-Abelian braiding of parafermions. Finally, in Sec. VI, we discuss the experimental parameters of the superconducting device for realizing our scheme and the potential application in high-dimensional topological quantum computing.

II. THE MODEL

We start by considering the \mathbb{Z}_d plaquette model on the two-dimensional square lattice with a checkerboard pattern [Fig. 1(a)]. On each vertex i , there is a qudit with d basis states $|m_i\rangle$ ($m_i = 0, 1, 2, \dots, d-1$). Physically, the qudit is realized by the intrinsic multi-level space of transmons. Their good coherence and sufficiently large anharmonicity allow transmons to function as qudits, with the lowest d energy levels encoding the qudit basis states [Fig. 1(b)]. The Hilbert space is spanned by the qudit states on all the vertices. The Hamiltonian is

$$H = - \sum_p O_p + h.c., \quad O_p = Z_1 X_2 Z_3^\dagger X_4^\dagger, \quad (1)$$

where the labels of the qudits are shown in the top of Fig. 1(a), and the sum of plaquettes p is for all the light and dark plaquettes. Here, Z , X , Z^\dagger , and X^\dagger are generalized Pauli operators. The generalized Pauli operators are defined by the properties: $X^d = \mathbb{1}$, $Z^d = \mathbb{1}$, $XZ = \omega ZX$, where $\omega = e^{\frac{2\pi i}{d}}$. They act on the qudit basis as $Z|m\rangle = \omega^m|m\rangle$ and $X|m\rangle = |m-1 \pmod{d}\rangle$. The experimental implementation of single-qudit operations uses a microwave drive resonant with specific subspaces of qudit states. For $d = 3$ (i.e., a qutrit), an arbitrary single-qutrit gate can be decomposed into operations within the two subspaces $\{|0\rangle, |1\rangle\}$ and $\{|1\rangle, |2\rangle\}$ [78, 81]. Accounting for the AC Stark effect due to anharmonicity helps

achieve high-fidelity single-qutrit gates [81, 82]. It is convenient to introduce a graphical representation [Fig. 1(a)] for the generalized Pauli operators and their commutation relations. With this representation, the stabilizer O_p is described by a loop operator around the plaquette p , which satisfies $O_p^d = 1$ and has eigenvalues $1, \omega, \dots, \omega^{d-1}$. Stabilizers on different plaquettes commute with each other; therefore, the Hamiltonian Eq. (1) is exactly solvable. The ground state $|\Psi_0\rangle$ satisfies

$$O_p |\Psi_0\rangle = O_p^\dagger |\Psi_0\rangle = |\Psi_0\rangle, \quad \forall p. \quad (2)$$

The elementary excitations of the Hamiltonian Eq. (1) are charge excitations e, e^2, \dots, e^{d-1} on light plaquettes, and flux excitations m, m^2, \dots, m^{d-1} on dark plaquettes [see Appendix. A for details]. More general excitations involve composites $e^k m^{d-k}$ of charge and flux excitations, known as dyons. These excitations are Abelian anyons and are created in pairs by string operators [as defined graphically in Fig. 1(a)].

To study non-Abelian statistics, we need to engineer dislocations. The dislocation in the square lattice that we consider is a one-dimensional extended object formed by tilting the edges along a line. Associated with the dislocation are two point-like defects at the ends, characterized by trivalent vertices on the pentagon plaquettes [Fig. 1(a)]. In the \mathbb{Z}_d plaquette model, the dislocation is engineered by deforming stabilizers O_p and $O_{p'}$ on two neighbouring plaquettes to a single stabilizer $O_{p'} O_p$ [Fig. 1(c)]. This deformation effectively removes the edge between the plaquettes and reduces the number of stabilizers by one. Therefore, N such dislocations result in a Nd -fold ground-state degeneracy, with each defect having a quantum dimension \sqrt{d} . This indicates the non-Abelian nature of the defect. These non-Abelian defects behave like parafermions. The underlying physics linking the defect to the parafermion is that the defect generates the electric-magnetic exchange symmetry. To illustrate this, we create an $e-\bar{e}$ charge pair by applying a Z gate to a qudit, and move the \bar{e} particle through the branch cut connecting two defects using a string operator [Fig. 1(a)]. The \bar{e} excitation transforms into the \bar{m} excitation, indicating an $e-m$ exchange. This shows that the defect identifies the dyon excitation $e^k m^{d-k}$ ($k = 1, 2, \dots, d-1$) with the trivial topological charge 1, giving rise to the following fusion rules:

$$\gamma \times \gamma = 1 + \sum_{k=1}^{d-1} e^k m^{d-k}, \quad (3)$$

where γ denotes the defects. Equation (3) is exactly the fusion rules of parafermions. For clarity, we henceforth refer to these defects as parafermions. By applying certain two-qudit gates, whose general forms are shown later, we can move the parafermions apart in space. This allows to realize the fusion and braiding of parafermions. Hereafter, we focus on the qutrit case, i.e., the \mathbb{Z}_3 plaquette model, for simplicity. Generalizing the methods to larger d is straightforward.

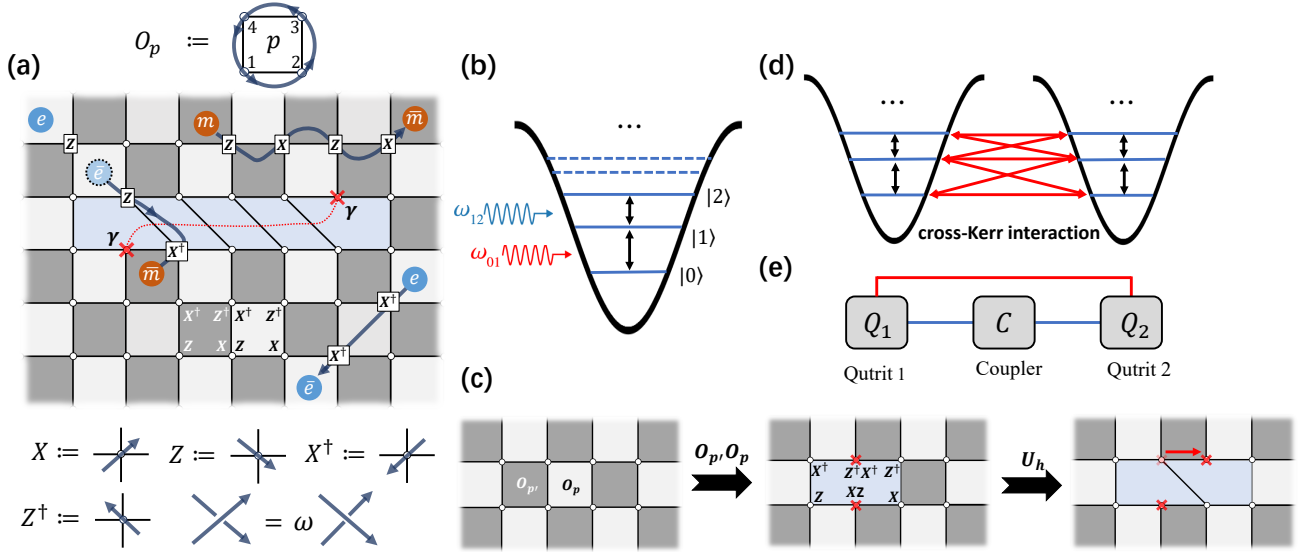


FIG. 1. Illustration of the model with a pair of prafermions. (a) The \mathbb{Z}_d plaquette model on an checkerboard lattice with a dislocation colored by light blue, where the small white dots represent qudits. The red cross marks the defect associated with the dislocation, identified as the parafermion mode γ . The red dotted line indicates the branch cut connecting the two parafermions. The arrowed dark blue curves represent string operators that create $e - \bar{e}$ and $m - \bar{m}$ excitations, which reside on the light and dark plaquettes, respectively. In our convention, the e or m particle is located at the start of the string operator. Stabilizers O_p on both dark and light plaquettes are shown. Graphical representation of the generalized Pauli operators, commutation relation, and stabilizers are shown. (b) An illustration of the energy diagram and microwave driving of a typical transmon as a multilevel system. The frequency difference $\omega_{12} - \omega_{01}$ characterizes the anharmonicity. (c) Dislocations are engineered by replacing two neighboring stabilizers with a single one. Applying a two-qudit quantum circuit moves and separates the parafermion defects. (d) Schematic of the cross-Kerr interaction that is used to realize two-qutrit gates. (e) A specific configuration for realizing the tunable cross-Kerr interaction using a frequency-tunable coupler between two fixed-frequency transmon qutrits.

III. GROUND STATE PREPARATION AND CREATION OF PARA-FERMIONS

In this section, we present methods to efficiently prepare the ground state of the stabilizer Hamiltonian in Eq. (1) on a planar surface. With the ground state, we show how parafermions can be created. For illustration, we focus on the case of $d = 3$, where the fundamental degrees of freedom are qutrits.

A. Ground state preparation

We consider the \mathbb{Z}_3 plaquette model with 6×6 qutrits [Fig. 2(a)]. The system is initially in the product state $|0\rangle^{\otimes 36}$. The ground state of the model is long-range entangled, which requires two-qutrit entangled operations for the preparation. This can be experimentally achieved through the tunable cross-Kerr interaction between two qutrits [Fig. 1(d)]. A specific configuration for this tunable coupling is shown in Fig. 1(e), where nearest-neighbor transmons are coupled via frequency-tunable couplers. Adjusting the coupler frequency modifies the strength of the cross-Kerr interaction, which, in combination with single-qutrit operations, enables the realization of efficient conditional phase gates [76]. Alternatively, the

differential AC Stark shift on two fixed-frequency transmon qutrits with static coupling can dynamically realize the conditional phase gate [79].

To prepare the ground state $|\Psi_0\rangle$ in Eq. (2), we first select a set of representative qutrits on light plaquettes [red dots in Fig. 2(b)] and apply the generalized Hadamard gate to them. The generalized Hadamard gate is defined by the quantum Fourier transform [53, 83]:

$$H^{(d)} |j\rangle = \frac{1}{\sqrt{d}} \sum_{i=0}^{d-1} \omega^{ij} |i\rangle. \quad (4)$$

In the case of qutrits, the generalized Hadamard gate acts on the state $|0\rangle$ as:

$$|+\rangle := H^{(3)} |0\rangle = \frac{1}{\sqrt{3}} (|0\rangle + |1\rangle + |2\rangle), \quad (5)$$

which is the common eigenstate of X and X^\dagger with eigenvalue 1. The generalized Hadamard gate can be implemented by decomposing the gate into time evolutions as $H^{(3)} = e^{-iH_d t} e^{-iH_o t}$, where $H_o = \sum_{i,j=0}^2 m_{ij} |i\rangle \langle j| + h.c.$ is off-diagonal, and $H_d = \text{diag}(\phi_0, \phi_1, \phi_2)$ is diagonal with complex parameters m_{ij} and real parameters ϕ_i . The generator H_o is experimentally realized by simultaneously microwave driving transitions between the three pairs of energy levels of the qutrit, while H_d is implemented by adjusting the phases of the drive pulses [84].

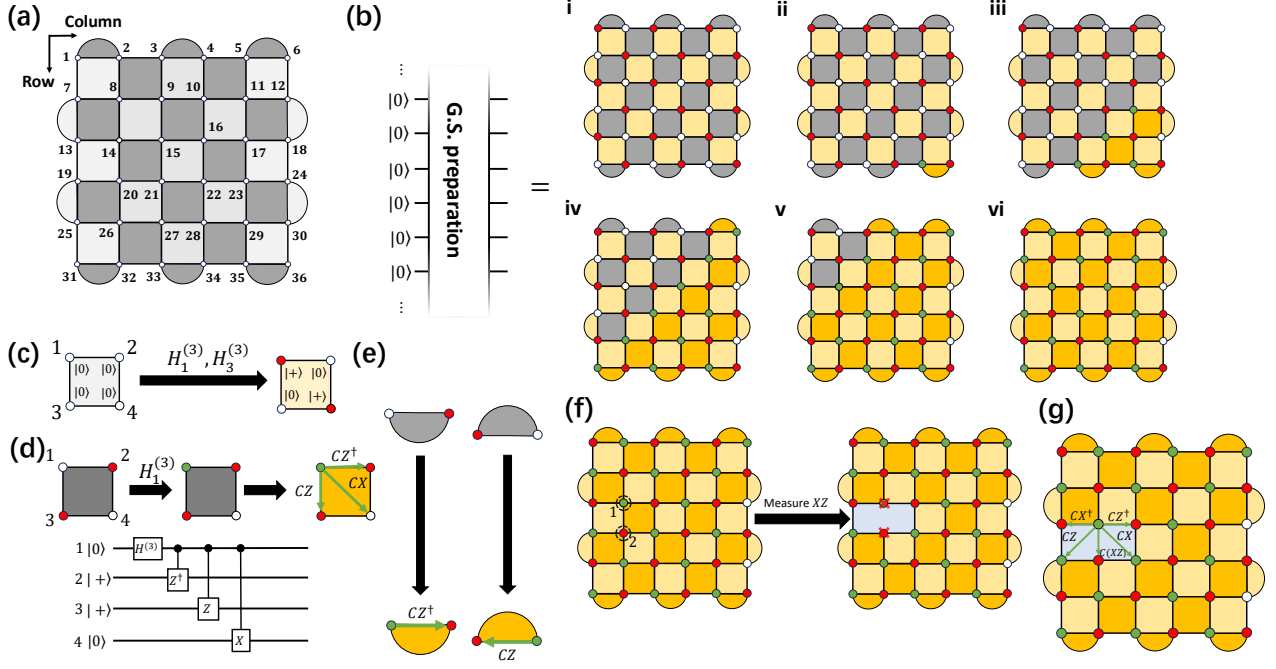


FIG. 2. Illustration of the ground state preparation and parafermion creation protocol. (a) The \mathbb{Z}_3 plaquette model with a 6×6 array of qutrits. (b) Explicit procedure for the ground state preparation. The system is initialized with all qutrits in $|0\rangle$. Red dots indicate the representative qutrits used to prepare the light plaquettes, while green dots represent the control qutrits used to apply conditional two-qutrit gates for preparing the dark plaquettes. The plaquettes in the ground state are colored pale yellow for light plaquettes and gold for dark plaquettes. (c) Applying the generalized Hadamard gate to the representative qutrits prepares the light plaquettes in the ground state. (d) A circuit is applied to the dark plaquettes to prepare them in the ground state. (e) Circuits for preparing boundary dark plaquettes in the ground state. (f) Measuring two neighboring qutrits creates a pair of parafermions. (g) An alternative method for creating parafermions involves ground state preparation on a lattice with a hole.

After applying the $H^{(3)}$ to each representative qutrit, all the light plaquettes (including the light boundary plaquettes) are prepared in the ground state [Fig. 2(c)]. Next, we select the control qutrit on each dark bulk plaquette [green dots in Fig. 2(b)] and apply CZ , CZ^\dagger , and CX gates to prepare all the dark plaquettes in the ground state [Figs. 2(d) and 2(e)]. The control two-qutrit gates must be applied layer by layer, ensuring that the state stored in the representative qutrits remains unchanged until the controlled operations on their respective plaquettes are applied. Ground state preparation on the dark plaquettes does not cause any light plaquette to deviate from the ground state, as their stabilizers commute with each other. In this way, we prepare the entire system in the ground state. The depth of the ground state preparation circuit depends linearly on the size of the lattice (\sqrt{n} in our set up, with n the number of qutrits).

An alternative, more efficient method exists if the system allows for non-destructive measurement for all plaquette states simultaneously. This requires appending an ancillary qutrit to each plaquette. We then use the generalized Hadamard test. More precisely, we first initialize all the ancillary qutrits in the $|+\rangle$ state, and the

total state on each plaquette is

$$|\Psi_{tot}\rangle = \frac{1}{\sqrt{3}} (|\tilde{0}\rangle + |\tilde{1}\rangle + |\tilde{2}\rangle) \otimes |\Psi_p\rangle, \quad (6)$$

where the $|\tilde{j}\rangle$ denotes the ancillary state, and $|\Psi_p\rangle$ denotes the plaquette state. Then we act O_p conditioned on the ancillary state, transforming the state to

$$\frac{1}{\sqrt{3}} (|\tilde{0}\rangle |\Psi_p\rangle + |\tilde{1}\rangle O_p |\Psi_p\rangle + |\tilde{2}\rangle O_p^\dagger |\Psi_p\rangle). \quad (7)$$

After applying a $H^{(3)}$ gate to each ancillary qutrit, we measure all the ancillary states at the same time to project each of them onto $|\tilde{0}\rangle$. The plaquette state transforms to

$$\frac{1}{3} (\mathbb{1} + O_p + O_p^\dagger) |\Psi_p\rangle = \Pi_p^0 |\Psi_p\rangle, \quad (8)$$

which means each plaquette is subjected to a ground-state projector and prepared in the ground state.

Fidelity of the ground state preparation can be characterized by a standard quantum state tomography (QST) method to reconstruct the state density matrix. The expectation value $\langle \Pi_p^0 \rangle$ of the ground state projector on

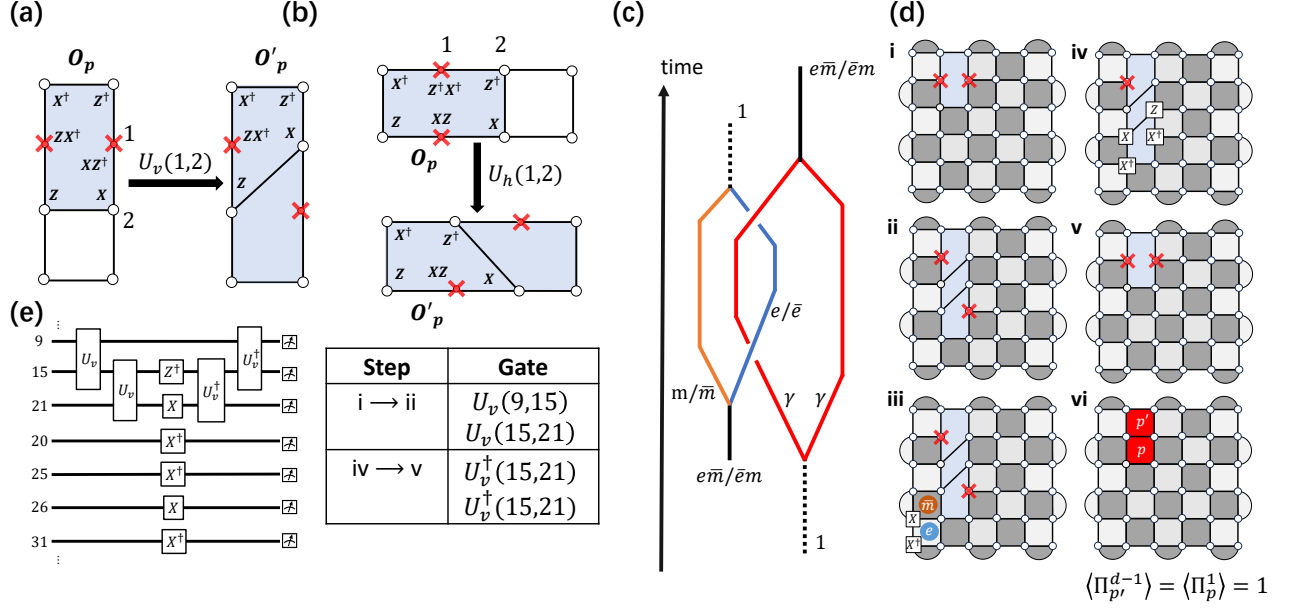


FIG. 3. Generalized code deformation and the fusion rules of parafermions. (a) Code deformation that moves the parafermion vertically. (b) Code deformation that moves the parafermion horizontally. (c) Illustration of the creation of a composite excitation and braiding e or \bar{e} with one parafermion. After the braiding, the excitations fuse to the trivial topological charge. (d) Explicit procedure for realizing the fusion of parafermions. Observables are characterized by $\langle \Pi_{p'}^{d-1} \rangle = \langle \Pi_p^1 \rangle = 1$ (e) Circuit and two-qutrit gates used in the procedure.

each plaquette can be computed from the density matrix. By repeating the experiment multiple times, one obtains the average value $\langle \Pi_p^0 \rangle$ for each plaquette. If $\langle \Pi_p^0 \rangle = 1$, it indicates perfect preparation of the ground state on the plaquette p ; if $\langle \Pi_p^0 \rangle < 1$, it indicates that the plaquette deviates from the ground state. This is the typical method used to characterize ground state preparation in digital simulations with superconducting qubits, and it can be easily extended to the qutrit case.

B. Parafermions creation

With the ground state prepared, we now proceed to create a pair of parafermions. To achieve this, we select two neighboring qutrits and measure them in the XZ basis if they are vertically adjacent or in the XZ^\dagger basis if they are horizontally adjacent. By measurement, we project the qutrits onto the eigenstate corresponding to the eigenvalue 1 of XZ or XZ^\dagger : $\frac{1}{\sqrt{3}}(|0\rangle + \omega|1\rangle + |2\rangle)$ for XZ , and $\frac{1}{\sqrt{3}}(|0\rangle + \omega|1\rangle + |2\rangle)$ for XZ^\dagger . Since XZ , XZ^\dagger , and their complex conjugates are creation operators of $e\bar{m} - \bar{e}m$ excitation pairs, this projection prepares the qutrits in the coherent state of these creation operators, effectively condensing the $e\bar{m}$ and $\bar{e}m$ excitations in the local region [the light blue region in Fig. 2(f)]. Because the two qutrits are projected separately, they are not directly entangled, which effectively removes the edge between them, thereby creating a pair of parafermions supported by the condensate [Fig. 2(f)].

An alternative method involves engineering a hole in the lattice [Fig. 2(g)], which can be physically realized by turning off the coupling between two neighboring transmons or a natural dislocation on the superconducting chip. With this imperfect lattice, we prepare the ground state as described in the previous subsection, but for the region with the hole, we apply a control- XZ gate to the corresponding qutrit. This creates a pair of parafermions with the stabilizer shown in Fig. 1(c).

IV. FUSION OPERATIONS OF THE GENERATED PARA-FERMIONS

In this section, we propose the scheme to study the fusion rules of parafermions. To do this, we need to separate two parafermions in space. This is achieved by applying two-qutrit unitary operators, which are derived from the generalized code deformation method. We begin by introducing this method and then, by combining it with string operators, we establish the protocol for realizing the fusion parafermions.

A. Generalized code deformation

Code deformation is a technique used to convert one error-correcting code into another by modifying the stabilizers, enabling fault-tolerant logical gate operations within surface codes [85, 86]. Beyond quantum infor-

mation science, code deformation also finds applications in condensed matter physics. Topological surface codes, such as the toric code, are rooted in topological quantum field theory, which provides the framework for topological orders. In this context, code deformation involves altering the topological structure of the field theory, such as engineering topological defects, to enrich the properties of topological orders [87]. While the method has been extensively studied in qubit systems, its application to qudit systems remains relatively unexplored. In this section, we introduce a generalized approach to code deformation in qudit systems. This generalization allows for the derivation of unitary operators for moving parafermions in superconducting circuits. Our work extends the theoretical framework of code deformation, enabling its application to broader studies of topological orders and fault-tolerant computations using qudit stabilizer codes.

Given a stabilizer O_p on the plaquette p and Hamiltonian $H = -\sum_p O_p + h.c.$, with the local ground state $|\psi\rangle$ satisfying $O_p |\psi\rangle = O_p^\dagger |\psi\rangle = |\psi\rangle$, after a code deformation, such as a change in the geometry of the lattice, the stabilizer changes to O'_p , and the corresponding local ground state is denoted by $|\psi'\rangle$. The new local ground state is related to the original one by a unitary operator U : $|\psi'\rangle = U |\psi\rangle$. For qutrits, the unitary operator is given by

$$U = \frac{1}{\sqrt{3}} (\mathbb{1} + O_p^\dagger O_p + O'_p O_p^\dagger). \quad (9)$$

For our purposes, we study the code deformations depicted in Fig. 3(a) and Fig. 3(b), where the former moves the parafermion vertically and the latter moves the parafermion horizontally. The associated unitary operators for these deformations are

$$U_v(i, j) = \frac{1}{\sqrt{3}} (\mathbb{1} + \omega Z_i^\dagger X_j + Z_i X_j^\dagger), \quad (10)$$

for the vertical move, and for the horizontal move:

$$U_h(i, j) = \frac{1}{\sqrt{3}} (\mathbb{1} + \omega Z_j X_i + Z_j^\dagger X_i^\dagger), \quad (11)$$

where i and j denote the initial and final positions of the parafermion, respectively, before and after the deformation. Both operators U_v and U_h are two-qutrit operators, and their matrices in the $Z_i \otimes Z_j$ basis are

$$U_v = \frac{1}{\sqrt{3}} \begin{pmatrix} 1 & \omega & 1 & 0 & 0 & 0 & 0 & 0 & 0 \\ 1 & 1 & \omega & 0 & 0 & 0 & 0 & 0 & 0 \\ \omega & 1 & 1 & 0 & 0 & 0 & 0 & 0 & 0 \\ 0 & 0 & 0 & 1 & 1 & \omega & 0 & 0 & 0 \\ 0 & 0 & 0 & \omega & 1 & 1 & 0 & 0 & 0 \\ 0 & 0 & 0 & 1 & \omega & 1 & 0 & 0 & 0 \\ 0 & 0 & 0 & 0 & 0 & 0 & 1 & \bar{\omega} & \bar{\omega} \\ 0 & 0 & 0 & 0 & 0 & 0 & \bar{\omega} & 1 & \bar{\omega} \\ 0 & 0 & 0 & 0 & 0 & 0 & \bar{\omega} & \bar{\omega} & 1 \end{pmatrix}, \quad (12)$$

and

$$U_h = \frac{1}{\sqrt{3}} \begin{pmatrix} 1 & 0 & 0 & \omega & 0 & 0 & 1 & 0 & 0 \\ 0 & 1 & 0 & 0 & \bar{\omega} & 0 & 0 & \bar{\omega} & 0 \\ 0 & 0 & 1 & 0 & 0 & 1 & 0 & 0 & \omega \\ 1 & 0 & 0 & 1 & 0 & 0 & \omega & 0 & 0 \\ 0 & \bar{\omega} & 0 & 0 & 1 & 0 & 0 & \bar{\omega} & 0 \\ 0 & 0 & \omega & 0 & 0 & 1 & 0 & 0 & 1 \\ \omega & 0 & 0 & 1 & 0 & 0 & 1 & 0 & 0 \\ 0 & \bar{\omega} & 0 & 0 & \bar{\omega} & 0 & 0 & 1 & 0 \\ 0 & 0 & 1 & 0 & 0 & \omega & 0 & 0 & 1 \end{pmatrix}. \quad (13)$$

The operator U_h is related to U_v by the circuit in Fig. 4(a), where the qutrit SWAP gate is implemented using the circuit in Fig. 4(b). Here, the $K^{(3)}$ gate is defined by $K^{(3)} |j\rangle = |3-j\rangle$, which can be decomposed into several X operators.

The two-qutrit gates U_h and U_v belong to the Clifford group, meaning that they can be implemented using gates from a set of universal qutrit gates. The specific implementation circuit depends on the set of native gate of the device and the chosen circuit optimization method. Since the matrix of the operator U_v is block diagonal (Eq. (12)), we can decompose it as

$$U_v = e^{-iH_d t} e^{-iH_o t}, \quad (14)$$

where

$$H_d = \sum_{j,k,l=0}^2 m_{jkl} |jk\rangle \langle jl| + h.c. \quad (15)$$

and $H_o = \text{diag}(\phi_1, \phi_2, \phi_3, \phi_4, \phi_5, \phi_6)$. The generators can then be implemented using microwave drives for single-qutrit transitions, tunable cross-Kerr interactions by adjusting the coupler frequency, and phase shifts of drive pulses. As multiple decompositions are possible, an optimization algorithm is required to select the optimal parameters m_{jkl} and ϕ_i for efficient implementations. Recently developed optimization algorithms can reduce the number of two-qutrit gates in the circuit [88], and machine learning techniques may further enhance this process. After the operator U_v is implemented, the operator U_h is obtained using the circuit in Fig. 4(a).

B. Realization of fusion for parafermions

We now present the protocol to realize the fusion for parafermions. The characteristic fusion rules for parafermions are:

$$\gamma \times \gamma = 1 + e\bar{m} + \bar{e}m, \quad (16)$$

which is a special case of Eq. (3). This rule indicates that the parafermion provides the fusion channels that identify the $e\bar{m}$ and $\bar{e}m$ excitations with the trivial topological charge 1. A related fusion rule is

$$\gamma \times e\bar{m}/\bar{e}m = 1, \quad (17)$$

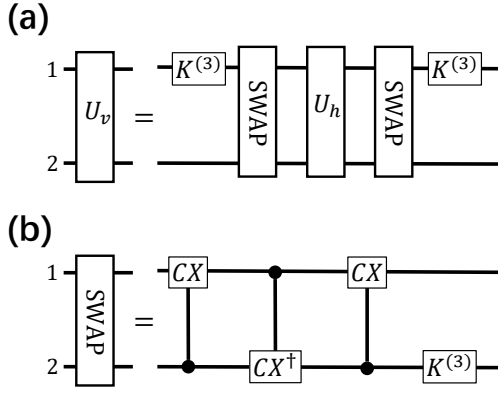


FIG. 4. (a) Circuit that relates two-qutrit operators U_v to U_h . (b) The qutrit SWAP circuit.

which shows that a parafermion absorbs either the $e\bar{m}$ or $\bar{e}m$ excitations. This can be achieved by braiding an e or \bar{e} excitation with a parafermion [Fig. 3(c)].

In Fig. 3(d), we explicitly show the procedure to realize fusions in Eqs. (16) and (17). The protocol begins by creating a pair of parafermions in the ground state and separating them using the operator U_v . Next, we create an $e\bar{m}$ dyon excitation by applying two local Pauli operators. The e excitation is then braided around one parafermion using a string operator, which consists of a sequence of Pauli operators. After braiding, the e excitation is transformed into the m excitation and proceeds to annihilate the \bar{m} excitation. Once this process is completed, we move the parafermion back to a neighboring position and measure the expectation values $\langle \Pi_{p'}^{d-1} \rangle$ and $\langle \Pi_p^1 \rangle$ by the QST method [the (vi) step in Fig. 3(d)], where p and p' denote the plaquettes supporting the dislocation. In the ground state, both $\langle \Pi_{p'}^{d-1} \rangle$ and $\langle \Pi_p^1 \rangle$ are zero. After the procedure, the parafermion absorbs the $e\bar{m}$ excitation, and thus we expect to observe $\langle \Pi_{p'}^{d-1} \rangle = 1$ and $\langle \Pi_p^1 \rangle = 1$. This procedure can be similarly applied to create and braid the $\bar{e}m$ excitation, providing an observable for experimental verification of the fusion rule in Eq. (17). To verify the fusion rule in Eq. (16), we reverse steps (iii-iv) in Fig. 3(d). In Fig. 3(e), we demonstrate the corresponding circuit and two-qutrit operators used in some steps of the procedure.

V. BRAIDING OF PARAFERMION MODES

After realizing the fusion of parafermions, we now turn to the braiding of them. To this end, we introduce the computational space basis encoded by parafermions, followed by the procedure for demonstrating the braiding of parafermions.

To encode information, a minimum number of four parafermions is required [Fig. 5(a)]. In this configuration, there are only two parity operators, $\Lambda_1 = \bar{\omega}\gamma_1\gamma_2^\dagger$

and $\Lambda_3 = \bar{\omega}\gamma_3\gamma_4^\dagger$ with γ the parafermion operator [see Appendix. B]. For convenience, the computational space is restricted to the two-dimensional subspace spanned by $\Lambda_1\Lambda_3 = 1$. With this restriction, four parafermions are sufficient to encode a logical qutrit. To find the basis of the computational space, we diagonalize the parity operator Λ_i and obtain the eigenstates $\{|0\rangle_\Lambda, |1\rangle_\Lambda, |2\rangle_\Lambda\}$. The logical qutrit state is defined by:

$$|\bar{j}\rangle = |j\rangle_{\Lambda_1} \otimes |3-j\rangle_{\Lambda_3}. \quad (18)$$

On the other hand, physically, the basis of the computational space is defined by the fusion tree of the four parafermions [Fig. 5(b)]. The specific transformation between the basis defined by the eigenstates of the parity operators and the fusion basis $|e\bar{m}/\bar{e}m\rangle_{\gamma_1\gamma_2} \otimes |\bar{e}m/e\bar{m}\rangle_{\gamma_3\gamma_4}$ requires selecting two base points on the lattice and constructing the parafermion operators using string operators whose start and end points are at these base points and satisfying the algebra in Eq. (B1) [3, 16]. Nevertheless, in this work, we do not make this exact transformation by selecting base points. Instead, we take a more direct approach to measure the braiding consequences of the parafermions, which does not rely on the relation between the fusion basis and the logical qutrit basis $|j\rangle_{\Lambda_1} \otimes |3-j\rangle_{\Lambda_3}$.

In the logical qutrit basis $\{|\bar{j}\rangle\}$, the half braiding operator U_2 that exchange γ_2 and γ_3 is an off-diagonal matrix, exhibiting the non-Abelian statistics. The matrix elements of U_2 are given by: $\langle \bar{i}|U_2|\bar{j}\rangle = \frac{1}{\sqrt{3}}c_{i-j}$, where $c_j = \omega^{\frac{j(j+5)}{2}}$. The full braiding matrix in the logical qutrit basis is

$$U_2^2 = \frac{1}{\sqrt{3}} \begin{pmatrix} i & i & \frac{2+\bar{\omega}}{\sqrt{3}} \\ \frac{2+\bar{\omega}}{\sqrt{3}} & i & i \\ i & \frac{2+\bar{\omega}}{\sqrt{3}} & i \end{pmatrix}, \quad (19)$$

and acts on the logical qutrit state $|\bar{0}\rangle$ as:

$$U_2^2 |\bar{0}\rangle = \frac{i}{\sqrt{3}} |\bar{0}\rangle + \frac{2+\bar{\omega}}{3} |\bar{1}\rangle + \frac{i}{\sqrt{3}} |\bar{2}\rangle. \quad (20)$$

The key point is that, regardless of how the logical states are identified in terms of the fusion basis, the fusion state corresponding to the trivial charge, $|1\rangle(\gamma_1 \times \gamma_2) \otimes |1\rangle(\gamma_3 \times \gamma_4)$, is always identified with the state $|\bar{0}\rangle$. Since the parafermions are created from the ground state, they are initially in the state $|\bar{0}\rangle$. After the full braiding of γ_2 and γ_3 , the state transforms as Eq. (20).

We now move on to the explicit procedure. In Fig. 5(d), we show the implementation of braiding of parafermions. The process begins by moving γ_3 to the bottom, followed by moving γ_2 to the right. After these steps, we move γ_2 back to its original position and finally return γ_3 to its starting point. After the braiding, the parafermions γ_1 and γ_2 fuse to form a composite excitation, denoted by f , which consists of the components 1, $\bar{e}m$, and $e\bar{m}$. Similarly, parafermions γ_3 and γ_4 fuse into

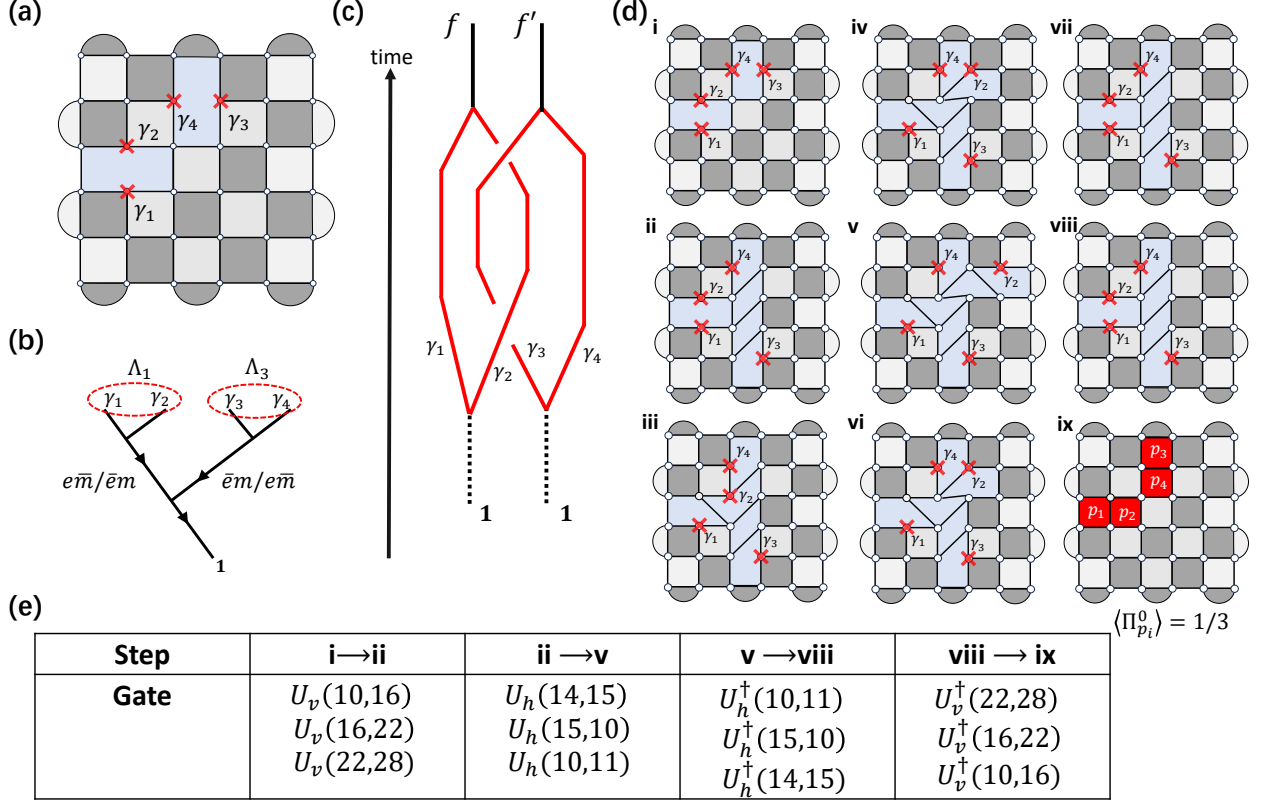


FIG. 5. Braiding of parafermion modes. (a) The \mathbb{Z}_3 plaquette model with four parafermions denoted by $\gamma_1, \gamma_2, \gamma_3$, and γ_4 labeled by the red crosses. (b) The fusion tree of parafermions. (c) Illustration of the creation of two pairs of parafermions from the ground state and braiding two of them. After the braiding, they fuse to two composite excitations denoted by f and f' , respectively. (d) Explicit procedure for the full braiding of parafermions γ_2 and γ_3 . (e) Two-qutrit gates used in the procedure.

another composite excitation f' [Fig. 5(c)]. In general, f and f' are distinct, but they are related by an electromagnetic transformation, where $e \leftrightarrow m$. According to Eq. (20), the probability of measuring the topologically trivial charge 1 from the composite excitation f or f' is always $\frac{1}{3}$. Therefore, when we measure the expectation value $\langle \Pi_p^0 \rangle$ using the QST method on the plaquettes that support the dislocation, we obtain $\langle \Pi_p^0 \rangle = \frac{1}{3}$. This provides an experimental observable for the braiding of parafermions. In Fig. 5(e), we show the two-qutrit gates used in this procedure.

VI. DISCUSSION AND OUTLOOK

Finally, we briefly discuss typical parameters for superconducting circuits to realize our scheme, particularly for the case of $d = 3$, and provide an outlook on the potential applications in high-dimensional topological quantum computing. One key parameter in superconducting circuits is the fidelity of single- and two-qutrit gates. Recent work has demonstrated the realization of the generalized Hadamard gate for qutrits, achieving a high fidelity of 0.992 [77]. More challenging is the implementation of

high-fidelity two-qutrit gates. In another recent study Ref. [79], the authors report the realization of CZ^\dagger and CZ gates for qutrits, with fidelities of 0.973 and 0.952, respectively. Since the fidelity of single-qutrit gates is much higher than that of two-qutrit gates, we will, as a first approximation, neglect errors from single-qutrit gates in the following analysis. Our ground state preparation protocol requires three two-qutrit gates for each dark plaquette. To achieve a ground state preparation fidelity of 0.90, the fidelity of the two-qutrit gates needs to be above 0.965, which is very close to the fidelity achievable with existing technology. Achieving higher level of fidelity would require further technological advances in superconducting devices, highlighting an important avenue for future research in this field. Other typical parameters include the relaxation time T_1 and the dephasing time T_2 , which must be sufficiently long to complete the braiding, fusion procedure, and measurement. Recent studies on transmon qutrits report T_1 values typically around $20\mu s$, with T_2 values around $10\mu s$ or higher [76, 79]. Considering that the gate times for high precision control are on the order of $10 - 100 ns$ for single-qutrit gates and $100 - 500 ns$ for two-qutrit gates, these parameters suggest that ground state preparation, along with subsequent fu-

sion and braiding procedures, is highly promising and achievable with current or near-future technology.

In the main text, we consider a 6×6 qutrit system for illustration, though this is not the minimal setup for our scheme. To study the fusion rules, a 3×4 qutrit setup is sufficient, while for braiding, a 4×4 setup is adequate. Reducing the number of qutrits in each row (or column) decreases the number of parafermion movement operations by two, saving the operation time by hundreds to thousands of nanoseconds. This reduction significantly enhances the success rate and fidelity of the experiment. The 6×6 example allows for quantum information processing based on more parafermions, such as 8 parafermions encoding two logical qutrits and their braiding. Additionally, considering braiding on well-designed quasi-one-dimensional configurations can further minimize the required number of qutrits.

Before concluding, we discuss the potential applications in high-dimensional quantum computing. Recent developments highlight several advantages over qubit-based quantum information processing [89] and flexible simulation of quantum dynamics [90]. Qudit versions of various quantum algorithms have already been developed [83, 91, 92]. High-dimensional quantum computing based on parafermion braiding is inherently fault-tolerant due to topological protection. While realizing parafermions in physical materials remains challenging, digital simulation may provide a feasible method for high-dimensional gate-based topological quantum computing in the near future. One exciting direction is demonstrating quantum algorithms in qudit systems using parafermions. Another challenge is using digital simulations of parafermions to implement the topologically protected CX gate, involving eight parafermions and twelve half-braidings.

In summary, we have proposed in this work an experimental scheme for realizing and manipulating non-Abelian parafermions in superconducting circuits, which is also applicable to other potential platforms. We demonstrate efficient protocols for ground state preparation and parafermion creation, along with methods for demonstrating fusion rules and braiding through experimental observables. Our work paves the way for the first digital simulation of parafermions and their braiding statistics in superconducting circuits.

ACKNOWLEDGMENTS

This work was supported by National Key Research and Development Program of China (2021YFA1400900), the National Natural Science Foundation of China (Grants No. 12425401 and No. 12261160368), the Innovation Program for Quantum Science and Technology (Grant No. 2021ZD0302000), and by Shanghai Municipal Science and Technology Major Project (Grant No. 2019SHZDZX01).

APPENDIX A: ELEMENTARY EXCITATIONS OF THE MODEL

In this section, we investigate the elementary excitations of the model Hamiltonian Eq. (1). The \mathbb{Z}_d plaquette model is an exactly solvable Hamiltonian model. Its spectrum includes a series of elementary excitations. To characterize them, we define the following projectors:

$$\Pi_p^\lambda = \frac{1}{d} \sum_{k=0}^{d-1} \omega^{\lambda(d-k)} O_p^k, \quad (\text{A1})$$

where $\lambda = 0, 1, \dots, d-1$. These projectors are observables $[\Pi_p^\lambda, H] = 0$ and satisfy

$$\sum_{\lambda} \Pi^\lambda = \mathbb{1}, \quad (\text{completeness}) \quad (\text{A2})$$

$$\Pi^\lambda \Pi^{\lambda'} = \delta_{\lambda\lambda'} \Pi^\lambda. \quad (\text{orthogonality}) \quad (\text{A3})$$

Therefore, their eigenvalues define a set of topological charges $\{\pi_p^0, \pi_p^1, \dots, \pi_p^\lambda, \dots, \pi_p^{d-1}\}$ for each plaquette p . In particular, the ground states have topological charge $\{1, 0, \dots, 0\}$.

Among the excitation states, we identify that states with topological charge $0, 1, \dots, 0$ on a given light (dark) plaquette p correspond to a charge (flux) excitation e (m) on p . Additional quantum numbers $\pi_p^\lambda = 1$ indicate the presence of a charge (flux) excitation e^λ (m^λ) on the light (dark) plaquette p . For convenience, we define $\bar{e} \equiv e^{d-1}$ and $\bar{m} \equiv m^{d-1}$. These elementary excitations can be created in pairs and moved via string operators. More generally, composite excitations are formed from these elementary excitations.

APPENDIX B: ALGEBRAIC THEORY OF PARA-FERMIONS AND BRAIDING OPERATOR

In this section, we introduce the algebraic theory of \mathbb{Z}_3 parafermions. For a general d , we refer to Ref. [54]. The algebraic relations for \mathbb{Z}_3 parafermions are given by:

$$\gamma_i \gamma_j = \omega^{\text{sgn}(j-i)} \gamma_j \gamma_i, \quad \gamma_i^3 = \mathbb{1}, \quad (\text{B1})$$

for an ordered set i , where $\omega = e^{\frac{2\pi i}{3}}$. To process quantum information, we need to consider N pairs of parafermions and unitary representations of the braid group B_{2N} . It turns out that there are six representations of the braid group in terms of the parity operators Λ_i , which are defined as:

$$\Lambda_i = \bar{\omega} \gamma_i \gamma_{i+1}^\dagger, \quad (\text{B2})$$

where $\bar{\omega}$ denotes the complex conjugate of ω . These operators satisfy the following relations:

$$\Lambda_i \Lambda_j = \Lambda_j \Lambda_i, \quad \text{if } |i-j| > 1 \quad (\text{B3})$$

$$\Lambda_i \Lambda_j = \omega^{\text{sgn}(j-i)} \Lambda_j \Lambda_i, \quad \text{if } |i-j| = 1 \quad (\text{B4})$$

The half-braiding operator that exchanges γ_i and γ_{i+1} is given by:

$$U_i = \frac{1}{\sqrt{3}} \sum_{m=0}^2 c_m (\Lambda_i)^m. \quad (\text{B5})$$

These operators must satisfy the Yang-Baxter equation:

$$U_i U_{i+1} U_i = U_{i+1} U_i U_{i+1}. \quad (\text{B6})$$

Solving the equation yields a family of six representations, which differ by the coefficients c_m :

$$c_m = \omega^{\pm \frac{m(m+2r+3)}{2}}, \quad r = 0, 1, 2. \quad (\text{B7})$$

In this paper, we focus on a specific representation where $c_m = \omega^{\pm \frac{m(m+5)}{2}}$, and the corresponding operator transformations under half-braiding are:

$$\gamma_i \mapsto \bar{\omega} \gamma_{i+1}, \quad (\text{B8})$$

$$\gamma_{i+1} \mapsto \gamma_i^\dagger (\gamma_{i+1})^2. \quad (\text{B9})$$

With this representation, the half-braiding operator U_i becomes:

$$U_i = \frac{1}{\sqrt{3}} \left(1 + \bar{\omega} \gamma_i \gamma_{i+1}^\dagger + \bar{\omega} \gamma_{i+1} \gamma_i^\dagger \right), \quad (\text{B10})$$

and the full braiding operator is obtained by squaring U_i^2 .

For a pair of \mathbb{Z}_3 parafermions, the computational basis, subject to the constraint $\Lambda_1 \Lambda_3 = 1$, is given by the eigenstates of the parity operators Λ_i :

$$\Lambda_i |m\rangle_{\Lambda_i} = m |m\rangle_{\Lambda_i}. \quad (\text{B11})$$

We denote the basis as $|\bar{k}\rangle = |k\rangle_{\Lambda_1} \otimes |3-k\rangle_{\Lambda_3}$ with $k = 0, 1, 2$. In this basis, the matrix representation of the half-braiding operator U_1 is diagonal:

$$U_1 = \sum_{k=0}^2 \tilde{c}_k |\bar{k}\rangle \langle \bar{k}|, \quad (\text{B12})$$

where $\tilde{c}_k = \frac{1}{\sqrt{3}} \sum_{j=0}^2 \omega^{jk} c_j$ is the Fourier transform of c_m . The half-braiding operator U_2 , however, is off-diagonal:

$$\langle \bar{k} | U_2 | \bar{l} \rangle = \langle \bar{k} | F^\dagger U_1 F | \bar{l} \rangle \quad (\text{B13})$$

$$= \frac{1}{\sqrt{3}} c_{k-l}, \quad (\text{B14})$$

$$= \frac{1}{\sqrt{3}} \omega^{\frac{(k-l)(k-l+5)}{2}}, \quad (\text{B15})$$

where F is the Fourier transformation operator defined by $F = \frac{1}{\sqrt{3}} \sum_{k,m=0}^2 \omega^{km} |\bar{k}\rangle \langle \bar{l}|$. Finally, we obtain the matrix of U_2^2 as in Eq. (19).

-
- [1] M. Aghaee, A. Alcaraz Ramirez, Z. Alam, R. Ali, M. Andrzejczuk, A. Antipov, M. Astafev, A. Barzegar, B. Bauer, J. Becker, U. K. Bhaskar, A. Bocharov, S. Boddapati, D. Bohn, J. Bommer, L. Bourdet, A. Bousquet, S. Boutin, L. Casparis, B. J. Chapman, S. Chatoor, A. W. Christensen, C. Chua, P. Codd, W. Cole, P. Cooper, F. Corsetti, A. Cui, P. Dalpasso, J. P. Dehollain, G. de Lange, M. de Moor, A. Ekefj rd, T. El Dandachi, J. C. Estrada Salda na, S. Fallahi, L. Galletti, G. Gardner, D. Govender, F. Griggio, R. Grigoryan, S. Grijalva, S. Gronin, J. Gukelberger, M. Hamdast, F. Hamze, E. B. Hansen, S. Heedt, Z. Heidarnia, J. Herranz Zamorano, S. Ho, L. Holgaard, J. Hornibrook, J. Indrapiromkul, H. Ingerslev, L. Ivancevic, T. Jensen, J. Jhoja, J. Jones, K. V. Kalashnikov, R. Kallaher, R. Kalra, F. Karimi, T. Karzig, E. King, M. E. Kloster, C. Knapp, D. Kocon, J. V. Koski, P. Kostamo, M. Kumar, T. Laeven, T. Larsen, J. Lee, K. Lee, G. Leum, K. Li, T. Lindemann, M. Looij, J. Love, M. Lucas, R. Lutchyn, M. H. Madsen, N. Madulid, A. Malmros, M. Manfra, D. Mantri, S. B. Markussen, E. Martinez, M. Mattila, R. McNeil, A. B. Mei, R. V. Mishmash, G. Mohandas, C. Mollgaard, T. Morgan, G. Moussa, C. Nayak, J. H. Nielsen, J. M. Nielsen, W. H. P. Nielsen, B. Nijholt, M. Nystrom, E. O'Farrell, T. Ohki, K. Otani, B. Paquelet W tz, S. Pauka, K. Petersson, L. Petit, D. Pikulin, G. Prawiroatmodjo, F. Preiss, E. Puchol Morejon, M. Rajpalke, C. Ranta, K. Rasmussen, D. Razmadze, O. Reentila, D. J. Reilly, Y. Ren, K. Reneris, R. Rouse, I. Sadovskyy, L. Sainiemi, I. Sanlorenzo, E. Schmidgall, C. Sfiligoj, M. B. Shah, K. Simoes, S. Singh, S. Sinha, T. Soerensen, P. Sohr, T. Stankevici , L. Stek, E. Stuppard, H. Suominen, J. Suter, S. Teicher, N. Thiagarajah, R. Tholapi, M. Thomas, E. Toomey, J. Tracy, M. Turley, S. Upadhyay, I. Urban, K. Van Hoogdalem, D. J. Van Woerkom, D. V. Viazmitinov, D. Vogel, J. Watson, A. Webster, J. Weston, G. W. Winkler, D. Xu, C. K. Yang, E. Yucelen, R. Zeisel, G. Zheng, J. Zilke, and M. A. Quantum (Microsoft Quantum), *Nature* **638**, 651 (2025).
- [2] Y.-H. Chen, B.-Z. Wang, T.-F. J. Poon, X.-C. Zhou, Z.-X. Liu, and X.-J. Liu, *Phys. Rev. Res.* **6**, L042054 (2024).
- [3] S. Xu, Z.-Z. Sun, K. Wang, L. Xiang, Z. Bao, Z. Zhu, F. Shen, Z. Song, P. Zhang, W. Ren, X. Zhang, H. Dong, J. Deng, J. Chen, Y. Wu, Z. Tan, Y. Gao, F. Jin, X. Zhu, C. Zhang, N. Wang, Y. Zou, J. Zhong, A. Zhang, W. Li, W. Jiang, L.-W. Yu, Y. Yao, Z. Wang, H. Li, Q. Guo, C. Song, H. Wang, and D.-L. Deng, *Chinese Physics Letters* **40**, 060301 (2023).
- [4] T. I. Andersen, Y. D. Lensky, K. Kechedzhi, I. K. Drozdov, A. Bengtsson, S. Hong, A. Morvan, X. Mi, A. Opremcak, R. Acharya, R. Allen, M. Ansmann, F. Arute, K. Arya, A. Asfaw, J. Atalaya, R. Babbush, D. Bacon, J. C. Bardin, G. Bortoli, A. Bourassa, J. Bo-

- vaird, L. Brill, M. Broughton, B. B. Buckley, D. A. Buell, T. Burger, B. Burkett, N. Bushnell, Z. Chen, B. Chiaro, D. Chik, C. Chou, J. Cogan, R. Collins, P. Conner, W. Courtney, A. L. Crook, B. Curtin, D. M. Debroy, A. Del Toro Barba, S. Demura, A. Dunsworth, D. Eppens, C. Erickson, L. Faoro, E. Farhi, R. Fatemi, V. S. Ferreira, L. F. Burgos, E. Forati, A. G. Fowler, B. Foxen, W. Giang, C. Gidney, D. Gilboa, M. Giustina, R. Gosula, A. G. Dau, J. A. Gross, S. Habegger, M. C. Hamilton, M. Hansen, M. P. Harrigan, S. D. Harrington, P. Heu, J. Hilton, M. R. Hoffmann, T. Huang, A. Huff, W. J. Huggins, L. B. Ioffe, S. V. Isakov, J. Iveland, E. Jeffrey, Z. Jiang, C. Jones, P. Juhas, D. Kafri, T. Khat-tar, M. Khezri, M. Kieferová, S. Kim, A. Kitaev, P. V. Klimov, A. R. Klots, A. N. Korotkov, F. Kostritsa, J. M. Kreikebaum, D. Landhuis, P. Laptev, K.-M. Lau, L. Laws, J. Lee, K. W. Lee, B. J. Lester, A. T. Lill, W. Liu, A. Locharla, E. Lucero, F. D. Malone, O. Mar-tin, J. R. McClean, T. McCourt, M. McEwen, K. C. Miao, A. Mieszala, M. Mohseni, S. Montazeri, E. Mount, R. Movassagh, W. Mruczkiewicz, O. Naaman, M. Neeley, C. Neill, A. Nersisyan, M. Newman, J. H. Ng, A. Nguyen, M. Nguyen, M. Y. Niu, T. E. O'Brien, S. Omonije, A. Petukhov, R. Potter, L. P. Pryadko, C. Quintana, C. Rocque, N. C. Rubin, N. Saei, D. Sank, K. Sankarago-mathi, K. J. Satzinger, H. F. Schurkus, C. Schuster, M. J. Shearn, A. Shorter, N. Shutty, V. Shvarts, J. Skruzny, W. C. Smith, R. Somma, G. Sterling, D. Strain, M. Szalay, A. Torres, G. Vidal, B. Villalonga, C. V. Heid-weiller, T. White, B. W. K. Woo, C. Xing, Z. J. Yao, P. Yeh, J. Yoo, G. Young, A. Zalcman, Y. Zhang, N. Zhu, N. Zobrist, H. Neven, S. Boixo, A. Megrant, J. Kelly, Y. Chen, V. Smelyanskiy, E.-A. Kim, I. Aleiner, P. Roushan, G. Q. Ai, and Collaborators, *Nature* **618** (2023), [10.1038/s41586-023-05954-4](https://doi.org/10.1038/s41586-023-05954-4).
- [5] G. Semeghini, H. Levine, A. Keesling, S. Ebadi, T. T. Wang, D. Bluvstein, R. Verresen, H. Pichler, M. Kalinowski, R. Samajdar, A. Omran, S. Sachdev, A. Vishwanath, M. Greiner, V. Vuletić, and M. D. Lukin, *Science* **374**, 1242 (2021), <https://www.science.org/doi/pdf/10.1126/science.abi8794>.
- [6] S. De Léséleuc, V. Lienhard, P. Scholl, D. Barredo, S. Weber, N. Lang, H. P. Büchler, T. Lahaye, and A. Browaeys, *Science* **365**, 775 (2019).
- [7] J. Nakamura, S. Liang, G. C. Gardner, and M. J. Manfra, *Nature Communications* **13**, 344 (2022).
- [8] J. Nakamura, S. Liang, G. C. Gardner, and M. J. Manfra, *Nature Physics* **16**, 931 (2020).
- [9] B. Rosenow, I. P. Levkivskiy, and B. I. Halperin, *Phys. Rev. Lett.* **116**, 156802 (2016).
- [10] R. HANBURY BROWN and R. Q. TWISS, *Nature* **178**, 1046 (1956).
- [11] H. Bartolomei, M. Kumar, R. Bisognin, A. Marguerite, J.-M. Berroir, E. Bocquillon, B. Plaçais, A. Cavanna, Q. Dong, U. Gennser, Y. Jin, and G. Fève, *Science* **368**, 173 (2020), <https://www.science.org/doi/pdf/10.1126/science.aaz5601>.
- [12] C. V. Kraus, P. Zoller, and M. A. Baranov, *Phys. Rev. Lett.* **111**, 203001 (2013).
- [13] C.-Y. Lu, W.-B. Gao, O. Gühne, X.-Q. Zhou, Z.-B. Chen, and J.-W. Pan, *Phys. Rev. Lett.* **102**, 030502 (2009).
- [14] H.-N. Dai, B. Yang, A. Reingruber, H. Sun, X.-F. Xu, Y.-A. Chen, Z.-S. Yuan, and J.-W. Pan, *Nature Communications* **13**, 1195 (2017).
- [15] C. Song, D. Xu, P. Zhang, J. Wang, Q. Guo, W. Liu, K. Xu, H. Deng, K. Huang, D. Zheng, S.-B. Zheng, H. Wang, X. Zhu, C.-Y. Lu, and J.-W. Pan, *Phys. Rev. Lett.* **121**, 030502 (2018).
- [16] H. Bombin, *Phys. Rev. Lett.* **105**, 030403 (2010).
- [17] A. Kitaev, *Annals of Physics* **321**, 2 (2006), january Special Issue.
- [18] A. Y. Kitaev, *Physics-uspekhi* **44**, 131 (2001).
- [19] D. A. Ivanov, *Phys. Rev. Lett.* **86**, 268 (2001).
- [20] J. Alicea, Y. Oreg, G. Refael, F. Von Oppen, and M. P. Fisher, *Nature Physics* **7**, 412 (2011).
- [21] J. Alicea, *Reports on progress in physics* **75**, 076501 (2012).
- [22] D. Aasen, M. Hell, R. V. Mishmash, A. Higginbotham, J. Danon, M. Leijnse, T. S. Jespersen, J. A. Folk, C. M. Marcus, K. Flensberg, *et al.*, *Phys. Rev. X* **6**, 031016 (2016).
- [23] V. Mourik, K. Zuo, S. M. Frolov, S. Plissard, E. P. Bakkers, and L. P. Kouwenhoven, *Science* **336**, 1003 (2012).
- [24] M. Deng, C. Yu, G. Huang, M. Larsson, P. Caroff, and H. Xu, *Nano letters* **12**, 6414 (2012).
- [25] L. P. Rokhinson, X. Liu, and J. K. Furdyna, *Nature Physics* **8**, 795 (2012).
- [26] A. Das, Y. Ronen, Y. Most, Y. Oreg, M. Heiblum, and H. Shtrikman, *Nature Physics* **8**, 887 (2012).
- [27] M.-X. Wang, C. Liu, J.-P. Xu, F. Yang, L. Miao, M.-Y. Yao, C. L. Gao, C. Shen, X. Ma, X. Chen, Z.-A. Xu, Y. Liu, S.-C. Zhang, D. Qian, J.-F. Jia, and Q.-K. Xue, *Science* **336**, 52 (2012).
- [28] H. Churchill, V. Fatemi, K. Grove-Rasmussen, M. Deng, P. Caroff, H. Xu, and C. M. Marcus, *Phys. Rev. B* **87**, 241401 (2013).
- [29] J.-P. Xu, C. Liu, M.-X. Wang, J. Ge, Z.-L. Liu, X. Yang, Y. Chen, Y. Liu, Z.-A. Xu, C.-L. Gao, D. Qian, F.-C. Zhang, and J.-F. Jia, *Phys. Rev. Lett.* **112**, 217001 (2014).
- [30] S. Nadj-Perge, I. K. Drozdov, J. Li, H. Chen, S. Jeon, J. Seo, A. H. MacDonald, B. A. Bernevig, and A. Yazdani, *Science* **346**, 602 (2014).
- [31] W. Chang, S. Albrecht, T. Jespersen, F. Kuemmeth, P. Krogstrup, J. Nygård, and C. M. Marcus, *Nature nanotechnology* **10**, 232 (2015).
- [32] S. M. Albrecht, A. P. Higginbotham, M. Madsen, F. Kuemmeth, T. S. Jespersen, J. Nygård, P. Krogstrup, and C. Marcus, *Nature* **531**, 206 (2016).
- [33] J. Wiedenmann, E. Bocquillon, R. S. Deacon, S. Hartinger, O. Herrmann, T. M. Klapwijk, L. Maier, C. Ames, C. Brüne, C. Gould, *et al.*, *Nature communications* **7**, 10303 (2016).
- [34] E. Bocquillon, R. S. Deacon, J. Wiedenmann, P. Leubner, T. M. Klapwijk, C. Brüne, K. Ishibashi, H. Buhmann, and L. W. Molenkamp, *Nature Nanotechnology* **12**, 137 (2017).
- [35] P. Zhang, K. Yaji, T. Hashimoto, Y. Ota, T. Kondo, K. Okazaki, Z. Wang, J. Wen, G. D. Gu, H. Ding, and S. Shin, *Science* **360**, 182 (2018).
- [36] D. Wang, L. Kong, P. Fan, H. Chen, S. Zhu, W. Liu, L. Cao, Y. Sun, S. Du, J. Schneeloch, R. Zhong, G. Gu, L. Fu, H. Ding, and H.-J. Gao, *Science* **362**, 333 (2018).
- [37] A. Fornieri, A. M. Whiticar, F. Setiawan, E. Portolés, A. C. Drachmann, A. Keselman, S. Gronin, C. Thomas, T. Wang, R. Kallagher, G. C. Gardner, E. Berg, M. J. Manfra, A. Stern, C. M. Marcus, and F. Nichele, *Nature*

- 569**, 89 (2019).
- [38] H. Ren, F. Pientka, S. Hart, A. T. Pierce, M. Kosowsky, L. Lunczer, R. Schlereth, B. Scharf, E. M. Hankiewicz, L. W. Molenkamp, B. I. Halperin, and A. Yacoby, *Nature* **569**, 93 (2019).
 - [39] B. Jäck, Y. Xie, J. Li, S. Jeon, B. A. Bernevig, and A. Yazdani, *Science* **364**, 1255 (2019).
 - [40] M. Aghaee, A. Akkala, Z. Alam, R. Ali, A. Alcaraz Ramirez, M. Andrzejczuk, A. E. Antipov, P. Aseev, M. Astafev, B. Bauer, J. Becker, S. Boddapati, F. Boekhout, J. Bommer, T. Bosma, L. Bourdet, S. Boutin, P. Caroff, L. Casparis, M. Cassidy, S. Chattoor, A. W. Christensen, N. Clay, W. S. Cole, F. Corsetti, A. Cui, P. Dalampiras, A. Dokania, G. de Lange, M. de Moor, J. C. Estrada Saldaña, S. Fallahi, Z. H. Fathabad, J. Gamble, G. Gardner, D. Govender, F. Grigio, R. Grigoryan, S. Gronin, J. Gukelberger, E. B. Hansen, S. Heedt, J. Herranz Zamorano, S. Ho, U. L. Holgaard, H. Ingerslev, L. Johansson, J. Jones, R. Kallaher, F. Karimi, T. Karzig, E. King, M. E. Kloster, C. Knapp, D. Kocon, J. Koski, P. Kostamo, P. Krogstrup, M. Kumar, T. Laeven, T. Larsen, K. Li, T. Lindemann, J. Love, R. Lutchyn, M. H. Madsen, M. Manfra, S. Markussen, E. Martinez, R. McNeil, E. Memisevic, T. Morgan, A. Mullally, C. Nayak, J. Nielsen, W. H. P. Nielsen, B. Nijholt, A. Nurmohamed, E. O’Farrell, K. Otani, S. Pauka, K. Petersson, L. Petit, D. I. Pikulin, F. Preiss, M. Quintero-Perez, M. Rajpalke, K. Rasmussen, D. Razmadze, O. Reentila, D. Reilly, R. Rouse, I. Sadovskyy, L. Sainiemi, S. Schreppler, V. Sidorkin, A. Singh, S. Singh, S. Sinha, P. Sohr, T. c. v. Stankevič, L. Stek, H. Suominen, J. Suter, V. Svidenko, S. Teicher, M. Temuerhan, N. Thiyagarajah, R. Tholapi, M. Thomas, E. Toomey, S. Upadhyay, I. Urban, S. Vaitiekėnas, K. Van Hoogdalem, D. Van Woerkom, D. V. Viazmitinov, D. Vogel, S. Waddy, J. Watson, J. Weston, G. W. Winkler, C. K. Yang, S. Yau, D. Yi, E. Yucelen, A. Webster, R. Zeisel, and R. Zhao (Microsoft Quantum), *Phys. Rev. B* **107**, 245423 (2023).
 - [41] C.-X. Liu, F. Setiawan, J. D. Sau, and S. D. Sarma, *Phys. Rev. B* **96**, 054520 (2017).
 - [42] S. Ahn, H. Pan, B. Woods, T. D. Stanescu, and S. D. Sarma, *Physical Review Materials* **5**, 124602 (2021).
 - [43] H. Pan and S. D. Sarma, *Phys. Rev. B* **103**, 224505 (2021).
 - [44] P. Yu, J. Chen, M. Gomanko, G. Badawy, E. Bakkers, K. Zuo, V. Mourik, and S. Frolov, *Nature Physics* **17**, 482 (2021).
 - [45] S. Takei, B. M. Fregoso, H.-Y. Hui, A. M. Lobos, and S. D. Sarma, *Phys. Rev. Lett.* **110**, 186803 (2013).
 - [46] C. Knapp, A. Chew, and J. Alicea, *Phys. Rev. Lett.* **125**, 207002 (2020).
 - [47] A. Kitaev, *Annals of Physics* **303**, 2 (2003).
 - [48] C. Nayak, S. H. Simon, A. Stern, M. Freedman, and S. Das Sarma, *Rev. Mod. Phys.* **80**, 1083 (2008).
 - [49] A. Ahlbrecht, L. S. Georgiev, and R. F. Werner, *Phys. Rev. A* **79**, 032311 (2009).
 - [50] M. Ezawa, *Phys. Rev. B* **110**, 045417 (2024).
 - [51] A. Benhemou, T. Angkhanawin, C. S. Adams, D. E. Browne, and J. K. Pachos, *Phys. Rev. Res.* **5**, 023076 (2023).
 - [52] C. Levaillant, B. Bauer, M. Freedman, Z. Wang, and P. Bonderson, *Phys. Rev. A* **92**, 012301 (2015).
 - [53] Y. Wang, Z. Hu, B. C. Sanders, and S. Kais, *Frontiers in Physics* **8** (2020), 10.3389/fphy.2020.589504.
 - [54] A. Hutter and D. Loss, *Phys. Rev. B* **93**, 125105 (2016).
 - [55] H. Anwar, E. T. Campbell, and D. E. Browne, *New Journal of Physics* **14**, 063006 (2012).
 - [56] S. Bravyi and A. Kitaev, *Phys. Rev. A* **71**, 022316 (2005).
 - [57] E. T. Campbell, H. Anwar, and D. E. Browne, *Phys. Rev. X* **2**, 041021 (2012).
 - [58] E. Cobanera and G. Ortiz, *Phys. Rev. A* **91**, 059901 (2015).
 - [59] U. Khanna, M. Goldstein, and Y. Gefen, *Phys. Rev. B* **105**, L161101 (2022).
 - [60] R. L. R. C. Teixeira and L. G. G. V. Dias da Silva, *Phys. Rev. B* **105**, 195121 (2022).
 - [61] N. Schiller, E. Cornfeld, E. Berg, and Y. Oreg, *Phys. Rev. Res.* **2**, 023296 (2020).
 - [62] K. Laubscher, D. Loss, and J. Klinovaja, *Phys. Rev. Res.* **2**, 013330 (2020).
 - [63] L. H. Santos, *Phys. Rev. Res.* **2**, 013232 (2020).
 - [64] K. Laubscher, D. Loss, and J. Klinovaja, *Phys. Rev. Res.* **1**, 032017 (2019).
 - [65] H. Ebisu, E. Sagi, Y. Tanaka, and Y. Oreg, *Phys. Rev. B* **95**, 075111 (2017).
 - [66] J. Klinovaja, A. Yacoby, and D. Loss, *Phys. Rev. B* **90**, 155447 (2014).
 - [67] J. Klinovaja and D. Loss, *Phys. Rev. B* **90**, 045118 (2014).
 - [68] J. Klinovaja and D. Loss, *Phys. Rev. Lett.* **112**, 246403 (2014).
 - [69] D. J. Clarke, J. Alicea, and K. Shtengel, *Nature Communications* **4**, 2041 (2013).
 - [70] J.-S. Hong, S.-Q. Zhang, X. Liu, and X.-J. Liu, *ArXiv:2403.09602* (2024).
 - [71] M. Barkeshli, C.-M. Jian, and X.-L. Qi, *Phys. Rev. B* **88**, 241103 (2013).
 - [72] Y.-Z. You and X.-G. Wen, *Phys. Rev. B* **86**, 161107 (2012).
 - [73] A. Blais, A. L. Grimsmo, S. M. Girvin, and A. Wallraff, *Rev. Mod. Phys.* **93**, 025005 (2021).
 - [74] S. Cao, M. Bakr, G. Campanaro, S. D. Fasciati, J. Wills, D. Lall, B. Shteynas, V. Chidambaram, I. Rungger, and P. Leek, *Quantum Science and Technology* **9**, 035003 (2024).
 - [75] T. Roy, Z. Li, E. Kapit, and D. Schuster, *Phys. Rev. Appl.* **19**, 064024 (2023).
 - [76] K. Luo, W. Huang, Z. Tao, L. Zhang, Y. Zhou, J. Chu, W. Liu, B. Wang, J. Cui, S. Liu, F. Yan, M.-H. Yung, Y. Chen, T. Yan, and D. Yu, *Phys. Rev. Lett.* **130**, 030603 (2023).
 - [77] M. A. Yurtalan, J. Shi, M. Kononenko, A. Lupascu, and S. Ashhab, *Phys. Rev. Lett.* **125**, 180504 (2020).
 - [78] A. Morvan, V. V. Ramasesh, M. S. Blok, J. M. Kreikebaum, K. O’Brien, L. Chen, B. K. Mitchell, R. K. Naik, D. I. Santiago, and I. Siddiqi, *Phys. Rev. Lett.* **126**, 210504 (2021).
 - [79] N. Goss, A. Morvan, B. Marinelli, B. K. Mitchell, L. B. Nguyen, R. K. Naik, L. Chen, C. Jünger, J. M. Kreikebaum, D. I. Santiago, J. J. Wallman, and I. Siddiqi, *Nature Communications* **13** (2022), 10.1038/s41467-022-34851-z.
 - [80] N. Goss, S. Ferracin, A. Hashim, A. Carignan-Dugas, J. M. Kreikebaum, R. K. Naik, D. I. Santiago, and I. Siddiqi, *npj Quantum Information* **10** (2024), 10.1038/s41534-024-00892-z.
 - [81] M. S. Blok, V. V. Ramasesh, T. Schuster, K. O’Brien,

- J. M. Kreikebaum, D. Dahlen, A. Morvan, B. Yoshida, N. Y. Yao, and I. Siddiqi, *Phys. Rev. X* **11**, 021010 (2021).
- [82] Q.-C. Liu, T.-F. Li, X.-Q. Luo, H. Zhao, W. Xiong, Y.-S. Zhang, Z. Chen, J. S. Liu, W. Chen, F. Nori, J. S. Tsai, and J. Q. You, *Phys. Rev. A* **93**, 053838 (2016).
- [83] C. Ye, P. Shi-Guo, Z. Chao, and L. Gui-Lu, *Communications in Theoretical Physics* **55**, 790 (2011).
- [84] J. L. O'Brien, G. J. Pryde, A. Gilchrist, D. F. V. James, N. K. Langford, T. C. Ralph, and A. G. White, *Phys. Rev. Lett.* **93**, 080502 (2004).
- [85] C. Vuillot, L. Lao, B. Criger, C. García Almudéver, K. Bertels, and B. M. Terhal, *New Journal of Physics* **21**, 033028 (2019).
- [86] H. Bombin, *New Journal of Physics* **13**, 043005 (2011).
- [87] Y. D. Lensky, K. Kechedzhi, I. Aleiner, and E.-A. Kim, *Annals of Physics* **452**, 169286 (2023).
- [88] D. Srinivasan, A. Beyer, D. Zhu, S. Churchill, K. Mehta, S. K. Sridhar, K. Chakrabarti, D. W. Steuerman, N. Chopra, and A. Dutt, "Trapped-ion quantum simulation of the fermi-hubbard model as a lattice gauge theory using hardware-aware native gates," (2024), [arXiv:2411.07778](https://arxiv.org/abs/2411.07778) [quant-ph].
- [89] E. T. Campbell, *Phys. Rev. Lett.* **113**, 230501 (2014).
- [90] M. Neeley, M. Ansmann, R. C. Bialczak, M. Hofheinz, E. Lucero, A. D. O'Connell, D. Sank, H. Wang, J. Wenner, A. N. Cleland, M. R. Geller, and J. M. Martinis, *Science* **325**, 722 (2009), <https://www.science.org/doi/pdf/10.1126/science.1173440>.
- [91] D. M. Nguyen and S. Kim, *International Journal of Theoretical Physics* **58** (2019), 10.1007/s10773-018-3910-4.
- [92] S. S. Ivanov, H. S. Tonchev, and N. V. Vitanov, *Phys. Rev. A* **85**, 062321 (2012).